Food Structure 49 (2026) 100548

Contents lists available at ScienceDirect

Food Structure

journal homepage: www.elsevier.com/locate/foostr

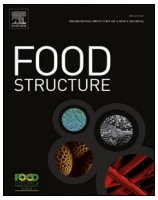

# Developing coating strategies for microaerogel beads to modulate bioactive release in foods

Lorenzo De Berardinis [a], Stella Plazzotta [a,*], Baldur Schroeter [b,c], Alberto Saitta [a], Irina Smirnova [b,c], Lara Manzocco [a]

[a] Department of Agricultural, Food, Environmental and Animal Sciences, University of Udine, Via Sondrio 2/A, Udine 33100, Italy
[b] Institute of Thermal Separation Processes, Hamburg University of Technology, Eißendorfer Straße 38, Hamburg 21073, Germany
[c] United Nations University Hub on Engineering to Face Climate Change at the Hamburg University of Technology, United Nations University Institute for Water, Environment and Health (UNU-INWEH), Hamburg, Germany

ARTICLE INFO

*Keywords:*
Controlled release
Ethylcellulose
Supercritical drying
Mesoporosity
Vanillin

ABSTRACT

The potential of aerogels, highly porous materials with an extensive surface area, to be used as ingredients able to load, protect and deliver bioactive compounds in food has recently attracted significant attention. However, the open-porosity of aerogels favours rapid absorption of both water and digestive fluids, triggering structural collapse and uncontrolled release of the loaded bioactives. In this study, a hydrophobic coating layer was used to finely modulate bioactive release from aerogels. To this aim, aerogel beads were prepared by gelling whey proteins at the isoelectric pH, followed by solvent exchange and supercritical-$CO_2$ drying. The resulting beads showed the typical whey protein microaerogel structure, with interconnected globular particles and a defined mesoporous network, providing a specific surface area of 27 $m^2/g$ estimated by QSDFT analysis, which was suitable for bioactive loading. The microaerogel beads were loaded with vanillin, selected as a representative bioactive molecule, and dip-coated in an ethylcellulose (EC) ethanolic solution at varying concentrations (1, 5, and 10 g/100 g). Coating application resulted in the formation of a protective coating layer, with thickness increasing with the EC concentration in the dipping solution, and this led to a marked reduction in the accessibility of microaerogel mesoporosity to $N_2$ sorption. Uncoated beads exhibited rapid Fickian diffusion of vanillin, while coating application shifted the transport mechanism toward a slower, barrier-controlled mass transfer. These results support aerogels as innovative food-grade delivery systems for controlled release of compounds with target functionalities in foods.

## 1. Introduction

Aerogels, recognised by IUPAC as the top emerging technology in chemistry in 2022 (IUPAC, 2022), are solid materials characterised by low density, high porosity, and extremely high internal surface area. These peculiar properties arise from the aerogel production process, which removes the solvent from a polymeric gel with a flow of $CO_2$ in the supercritical state. This technology allows the initial polymeric network to be preserved due to the low capillary forces involved during drying (García-González et al., 2019).

When supercritical-$CO_2$ drying is applied to biobased hydrogels, such as those made from carbohydrates and proteins, bioaerogels are obtained. In this case, a solvent exchange from water to ethanol (EtOH) is required before drying to reduce system polarity, resulting in an alcolgel whose continuous phase is highly soluble in $CO_2$. Bioaerogels are particularly appealing in a wide range of life-science fields, including pharmaceutical, environmental, and food sectors (Manzocco et al., 2021). In the food sector, these materials have the potential to be used as functional food ingredients able to load and deliver bioactive compounds through the diet (Ahmadi et al., 2016; de Oliveira et al., 2020; Kleemann et al., 2020; Ubeyitogullari & Ciftci, 2019). In fact, the open porosity and high internal surface area of aerogels allow them to load high amounts of the target molecule. Loading is generally achieved by wet or post-drying impregnation. For wet impregnation, the target molecule can be simply added to the aqueous or ethanol solution used for hydrogel and alcogel preparation, respectively. When supercritical-$CO_2$ drying is then performed, the target molecule precipitates within the aerogel pores *via* an antisolvent mechanism (Miguel et al.,

* Corresponding author.
*E-mail address:* stella.plazzotta@uniud.it (S. Plazzotta).

https://doi.org/10.1016/j.foostr.2026.100548
Received 15 January 2026; Received in revised form 23 June 2026; Accepted 25 June 2026
Available online 27 June 2026

2006). For example, Comin et al. (2012) loaded flax oil into β-glucan-based aerogels by mixing it with the aqueous phase used to prepare the initial hydrogel, leading to systems containing up to 10 g oil/100 g. Similarly, dos Santos et al., (2020) incorporated up to 0.77 g of resveratrol per g of alginate aerogels after solubilising the target molecule in ethanol during the solvent-exchange procedure. In post-drying impregnation, target molecule loading can be obtained by immersing the aerogel in a fluid containing the target molecule. In this context, κ-carrageenan and whey protein-based aerogels showed a remarkable capacity to absorb liquid oil, leading to systems containing up to 85 g oil/100 g (Jung et al., 2023; Manzocco et al., 2017, 2022; Plazzotta et al., 2020, 2021). Moreover, the loading of liquid oil in whey protein aerogel was demonstrated to significantly affect lipid digestibility (Plazzotta et al., 2022). Alternatively, impregnation can be performed using a supercritical-$CO_2$ solution saturated with the target molecule. In this case, the loading of the target molecule is driven by its chemical adsorption onto the aerogel pore surfaces, as well as by capillary condensation and local precipitation upon depressurisation (Smirnova & Gurikov, 2018). For instance, Ubeyitogullari and Ciftci (2017) used the supercritical-$CO_2$ impregnation approach to load nanoporous starch aerogels with crude phytosterols (99 mg phytosterols/g aerogel). In a subsequent work, Ubeyitogullari and Ciftci (2019) used aerogels loaded with phytosterols in the formulation of low-fat granola bars, revealing an increase in phytosterol bioaccessibility from 16% to 53%. With the same approach, Selmer et al. (2019) impregnated whey protein-based aerogel microparticles with fish oil rich in ω−3 fatty acids (0.74 g oil/g aerogel). The obtained results showed a reduced oxidation of fish oil upon 12-week storage. Similarly, fish oil was supercritically impregnated into aerogels based on whey proteins, egg white proteins and sodium caseinate, leading to systems containing up to 63 g oil/100 g. The loaded aerogels, tested for *in-vitro* digestion, showed high resistance to peptic digestion, retarding the release of the encapsulated fish oil in the intestinal tract (Kleemann et al., 2020). More recently, vanillin was efficaciously impregnated in cellulose and pectin-based aerogel particles, reaching a loading capacity in the range 10–60 g vanillin/100 g loaded aerogel (Méndez et al., 2023; Schroeter et al., 2021).

Nevertheless, the open structure of aerogels could represent an issue for their application as delivery systems for bioactive molecules in food. While aerogel porosity is needed for loading target molecules, it makes the aerogel structure highly susceptible to moisture adsorption, which might induce structural collapse and uncontrolled bioactive release. It has been demonstrated that whey protein aerogels, when stored at humidity (ERH) higher than 80% for 48 h, shift from a glassy to a rubbery state, losing porosity (Manzocco et al., 2022). Similarly, κ-carrageenan-based aerogels were demonstrated to collapse significantly when kept at an ERH exceeding 60% (Manzocco et al., 2017). Structural modification is expected to significantly accelerate when aerogels come into contact with water in a food product. In this context, whey protein, egg white protein and sodium caseinate aerogels exhibited a notable increase in volume upon absorption of aqueous media (Kleemann et al., 2020; Manzocco et al., 2022). Conversely, κ-carrageenan aerogels were found to completely solubilise when immersed in water (Manzocco et al., 2017). Additional aerogel interaction with aqueous environments inevitably occurs during digestion. In this context, it was demonstrated that protein aerogels significantly swelled during digestion, further steering the release of loaded molecules (Kleemann et al., 2020; Plazzotta et al., 2022).

Applying a coating to the surface of aerogels could be a promising solution to overcome the uncontrolled release of the loaded bioactive molecules. In this regard, the use of edible surface layers is a key aspect to be considered in the development of aerogels intended as delivery systems in foods. Goslinska et al. (2019) demonstrated that whey protein aerogels can be coated with an alcoholic solution of shellac, which crystallises directly onto the aerogel surface as the solvent evaporates, forming a coating layer that does not affect the inner porous structure of the aerogels. Schroeter et al. (2021) used shellac to coat cellulose aerogel particles loaded with vanillin and demonstrated that the thickness of the coating layer can efficaciously steer *in-vitro* vanillin release. In our recent work, whey protein aerogels were coated with three different edible coating agents, i.e., alginate, agar, and ethylcellulose (EC). EC was shown to be a particularly efficient barrier against moisture and water vapour absorption (De Berardinis et al., 2024b).

The present research focuses on further studying the feasibility of coating whey protein aerogels with an EC layer to control the release of loaded bioactive molecules. Vanillin was selected because it is widely used in food and beverages, owing to its aroma profile and health benefits (Olatunde et al., 2022), but its direct incorporation in food products is often impaired by high volatility and rapid degradation (Almeida et al., 2019). The possibility of controlling the release of vanillin by using the peculiar properties of coated aerogels would thus be highly appealing. To this aim, whey protein aerogel beads were loaded with vanillin and coated by dipping in ethylcellulose solutions at different concentrations (1, 5, or 10 g/100 g). The beads were characterised for their microstructure and physical properties (density, internal surface area, and coating thickness). The effect of coating on vanillin release in an aqueous environment was then evaluated. Modelling parameters of *in vitro* vanillin release were finally discussed to show the potential of aerogel coating for controlled delivery in food systems.

## 2. Materials and Methods

### 2.1. Microaerogel beads preparation

Whey protein isolate (WP, Davisco Foods International Inc., Le Seur, MN, United States) was dispersed in bi-distilled water (System advantage A10®, Millipore S.A.S, Molsheim, France) at 20 g/100 g, and stirred overnight at 4 °C. The protein solution was adjusted to the isoelectric point (pH 5) (pH-Meter BASIC 20, Crison, Barcelona, Spain) with 1 M HCl (Sigma Aldrich, Milan, Italy) and extruded from a 5 mL syringe into a coagulation bath containing sunflower oil at 85 °C. The syringe was held about 5 cm above the surface of the coagulation bath, while the oil was kept moving to prevent the droplets from adhering to the bottom of the bath before fully gelling. WP gelled droplets were collected with a filter and subjected to a water-to-ethanol solvent exchange procedure by immersion in ethanol (99.9 mL/100 mL, Carl Roth, Karlsruhe, Germany) until reaching an ethanol concentration equal to or higher than 98 mL/100 mL. The obtained alcogel beads were supercritically dried under continuous $CO_2$ flow (120–140 g/min). After the target temperature and pressure were reached, drying was performed at 60 °C and 120 bar for 3 h, and these conditions were maintained until complete ethanol extraction, followed by slow depressurization at 2 bar/min. The obtained aerogel beads, hereafter referred to as microaerogel beads, exhibited an average diameter of approximately 3 mm, as determined from measurements of 20 individual beads using a CD−15APXR digital caliper (Absolute AOS Digimatic, Mitutoyo Corporation, Kanagawa, Japan).

### 2.2. Supercritical-$CO_2$ impregnation of microaerogel beads

The microaerogel beads were inserted in filter bags and placed in a 250 mL autoclave for supercritical-$CO_2$ impregnation. Vanillin powder was positioned in an open metal cup at the base of the autoclave, in an aerogel-to-vanillin weight ratio of 1.0:1.5. Supercritical-$CO_2$ impregnation was conducted at 60 °C and 125 bar for 16 h. Following gradual depressurisation at a rate of 1 bar/min, the impregnated beads were collected. The total amount of vanillin loaded was determined based on the weight of the sample before and after supercritical-$CO_2$ impregnation.

### 2.3. Coating of microaerogel beads

An ethylcellulose (EC) coating solution was prepared according to De Berardinis et al. (2024b), with some modifications. Specifically, an EC 100 cp (ETHOCEL™ Standard 100 FP Premium, Dow Chemical, Midland, United States) was dissolved in absolute ethanol at increasing concentrations (1, 5, and 10 g/100 g) at 75 °C for 30 min under stirring until use. The microaerogel beads were held by metal clips and dipped for 3 s in the coating solution, corresponding to the minimum time required for manual handling and complete immersion. This operation was repeated twice, with the second dipping cycle enabling coating of the areas that were shielded by the metal clips during the first dip, thus ensuring complete coverage of the bead surface. The coated beads were placed on a mesh at room temperature under a laboratory hood for 1 h, to allow both coating setting and ethanol evaporation. Coated beads were stored in desiccators containing $P_2O_5$ at room temperature until use.

### 2.4. Characterization of microaerogel beads

#### 2.4.1. Appearance

Images were acquired using an image acquisition cabinet (Immagini & Computer, Bareggio, Italy) equipped with a digital camera (EOS 550D, Canon, Milano, Italy). The latter was positioned on an adjustable stand, positioned 50 cm above a black cardboard base, where the samples were positioned. Lighting was provided by 4 × 100 W frosted photographic floodlights, arranged to minimize shadow and glare.

#### 2.4.2. Scanning electron microscopy

The internal structure of the microaerogels and the thickness of the EC coatings were analyzed using scanning electron microscopy (SEM, Zeiss Supra VP55, Jena, Germany). Both intact and sectioned beads were coated with a thin layer of gold using a Sputter Coater SCD 050 (BAL-TEC) before the analysis. The measurements were carried out under a high vacuum, with an accelerating voltage of 2–5 kV using an in-lens detector.

#### 2.4.3. Volume and density

Microaerogel bead volume was calculated from the measured bead diameter, assuming a spherical geometry. Network density was calculated as the ratio of the weight of microaerogel beads and their volume, and expressed as g/cm$^3$. Measurements were carried out in triplicate.

#### 2.4.4. Specific surface area

Low-temperature $N_2$ adsorption–desorption analysis was performed using a Nova 3000e Surface Area Analyzer (Quantachrome Instruments, Boynton Beach, USA). For each analysis, ~ 25 mg of total sample mass was used. The specific surface area and mesopore volume were estimated using a QSDFT model under the assumption of cylindrical pores *via* double determinations. The samples were degassed under vacuum at 60 °C for at least 6 h prior to measurements.

#### 2.4.5. Static water contact angle

Static contact angles were measured using a drop shape analyzer (OCA 15EC, DataPhysics Instruments GmbH, Filderstadt, Germany). Water droplets with a volume of 1 μL were deposited onto the sample surface, and the contact angles were recorded immediately after deposition. To assess droplet penetration into the surface, the droplet was left in place and the contact angle was monitored over time until complete disappearance (up to 18 min). Measurements were carried out in triplicate with individual samples.

#### 2.4.6. Vanillin release experiments

Vanillin release experiments were carried out as previously described by Schroeter et al. (2021). Specifically, 5 impregnated microaerogel beads were placed in a beaker containing 500 g of demineralized water and gently stirred at 30 °C (stirring rate = 3, C-MAG HS10 hot-plate magnetic stirrer, Ika Werke, Staufen im Breisgau, Germany). Water was periodically collected (2 mL each time) and transferred to 1 cm path-length cuvettes. The vanillin concentration was measured using UV–Vis spectroscopy (Shimadzu UV−2501PC, UV–Vis recording spectrophotometer, Shimadzu Corporation, Kyoto, Japan) at a wavelength of 230 nm. After measurement, the sample solutions were returned to the beaker. Measurements were carried out in triplicate for the pristine sample and those treated with 1 g EC/100 g EtOH, 5 g EC/100 g EtOH. For the sample coated with the highest EC concentration (10 g EC/100 g EtOH), release measurements were carried out in duplicate due to limited sample availability; these data were used to support the concentration-dependent trend and were interpreted with caution.

### 2.5. Data analysis

The results are presented as mean values with standard deviations. Statistical analysis was performed using R v. 2.15.0 (The R Foundation for Statistical Computing). Bartlett's test was used to assess the homogeneity of variance. One-way ANOVA was conducted, followed by Tukey's *post hoc* test to identify statistically significant differences among the means ($p < 0.05$).

## 3. Results and Discussion

### 3.1. Microaerogel beads

The first part of the present study focused on characterising aerogel beads obtained upon water removal from WP hydrogel spheres *via* solvent exchange and supercritical drying. Fig. 1 reports the appearance of the hydrogel spheres and the resulting dried beads.

Following gelation, millimetre spheres with a roundish shape were efficaciously prepared (Fig. 1, a). The beads showed a diameter of 3.00 ± 0.01 mm and a white appearance, typical of the formation of microgels when WP are gelled at the isoelectric point (Nicolai, 2016). Upon supercritical-$CO_2$ drying, the beads preserved their roundish shape and dimension (Fig. 1, b) due to the low capillary forces involved during the applied process (García-González & Smirnova, 2013). Moreover, the beads showed a particularly white appearance, which can be attributed to the intense light scattering typical of highly porous materials, with characteristic pore or scatterer sizes comparable to or larger than visible wavelengths (Betz et al., 2012; Manzocco et al., 2022). In line with previous results (De Berardinis et al., 2024a), the microaerogel beads showed a low density (0.03 ± 0.01 g/cm$^3$). The $N_2$ physisorption isotherms recorded at 77 K exhibited a type IV characteristic with a very narrow hysteresis loop (Fig. 1, c). The hysteresis shape indicated a largely reversible adsorption–desorption behaviour (Thommes et al., 2015) and is consistent with adsorption in open, interparticle mesoporous networks. The corresponding pore size distribution (Fig. 1, c, inset) showed a pronounced maximum at a pore diameter of approximately 6 nm. A quantitative BET analysis was not used as a primary surface area descriptor since no sufficiently stable linear region or robust compliance with the BET selection criteria (e.g., consistent monolayer capacity and positive C values) could be identified within the conventional BET pressure range ($p/p_o$ ~ 0.05–0.30), which is typical for biopolymer-based, structurally heterogeneous aerogels. Instead, the specific surface area was estimated as a model-dependent "apparent" DFT-derived surface area obtained from a QSDFT analysis of the adsorption branch (pore model and assumption of cylindrical pores). The resulting surface area (27 ± 8 m$^2$/g) and mesopore volume (0.07 ± 0.02 cm$^3$/g) values were in the lower range, typical for whey protein-based aerogels produced *via* thermal gelation at the isoelectric point (Plazzotta et al., 2021).

SEM micrographs revealed an open-porous architecture (Fig. 1, d, e), characterised by the presence of a particulate, macroporous network of

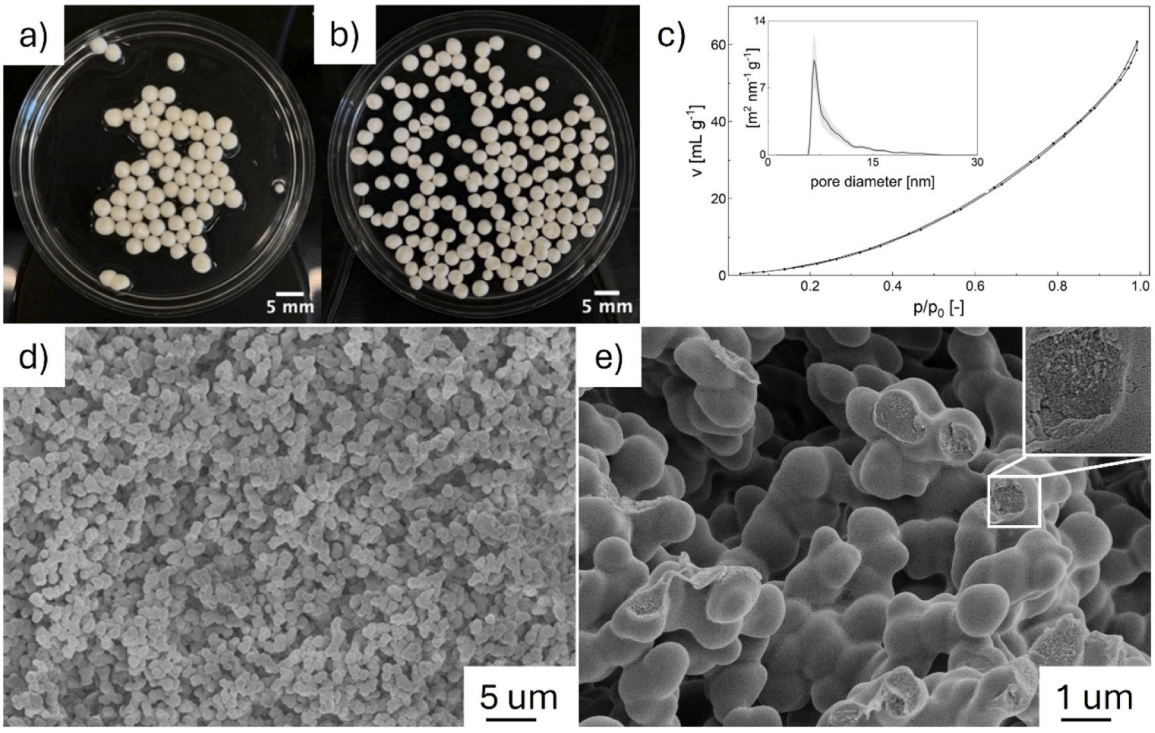


**Fig. 1.** Optical appearance of hydrogel (a) and microaerogel (b) beads. c) Nitrogen physisorption isotherm of pristine microaerogel beads. Inset: averaged pore size distribution estimated via QSDFT model (n = 2). The highlighted area represents the standard deviation. (d), (e) SEM images of the inner bead microstructure at different magnifications (5000 × and 25000 ×). Inset: inner part of an individual microaerogel, high resolution image (250000 ×).

interconnected spherical aggregates, known as microaerogels, obtained by supercritical-$CO_2$ drying of protein gels formed in the isoelectric pH region (Ciufarrin et al., 2024; De Berardinis et al., 2024b; Manzocco et al., 2022). Small mesopores were visible in the inner part of individual

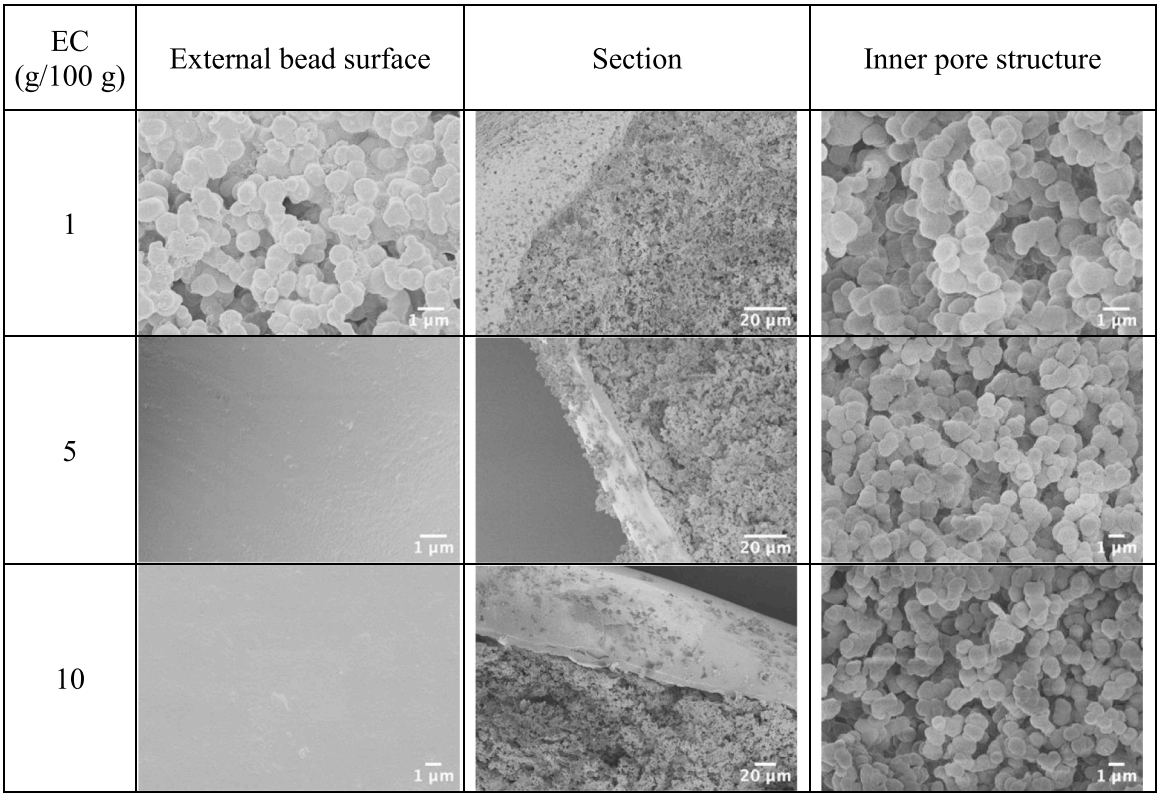


**Fig. 2.** Microstructure of surface, transversal section and inner part of microaerogel beads (representative images) coated by dipping in ethylcellulose solutions (EC) at increasing concentration (1, 5, 10 g/100 g).

microaerogels at higher magnifications (Fig. 1, e, inset).

### 3.2. Coating of microaerogel beads

The microaerogel beads were dip-coated in solutions containing increasing EC concentrations. Dipping did not affect bead shape and dimension, and the macroporous network formed by microaerogels remained intact as observed in the SEM images. In particular, Fig. 2 reports the microstructures of the surface, transversal section, and inner part of the coated beads.

The concentration of the EC coating solution had a significant impact on the coating layer appearance and thickness. The low viscosity of 1 g/100 g EC coating solution allowed the formation of a thin EC layer adhering to the surface of the single protein microaerogels, so that a continuous and uniform external shell was not observed on the surface of the beads. The coating layer onto microaerogels was expected to remain thinner than ~1 μm, as the deposited EC structures did not exceed the size of the underlying microaggregates. By contrast, when beads were dipped into the EC solutions at higher concentrations (5 and 10 g/100 g) and thus higher viscosity, even, smooth and completely enclosed coating layers were obtained. In this case, the microaerogel structure was no longer evident on the bead surface, which was well covered by coating layers of 1.9 ± 0.3 μm and 6.7 ± 0.7 μm thickness for the EC solutions at 5 and 10 g/100 g, respectively. To evaluate the ability of the coating layers to induce liquid water repellence, static water contact angle measurements were performed. Initial contact angles (Fig. 3a-c) were recorded immediately after droplet deposition. For the uncoated control sample, the water droplet was instantaneously absorbed into the bead matrix, preventing the acquisition of measurable data. In contrast, all coated beads exhibited initial static water contact angles in the range of approximately 96–131° (averaged values of replicates obtained from three individual samples: 1 g EC/100 g EtOH = 121 ± 8°, 5 g EC/100 g EtOH = 102 ± 8°, 10 g EC/100 g EtOH = 102 ± 4°). Notably, this behaviour was also observed for the sample coated with 1 g/100 g EC solution, despite the absence of a continuous, fully enclosed EC outer shell. This indicates that even a thin coating on the surface of individual microaerogels is sufficient to impart liquid water repellence. Monitoring the contact angle over a period of 3 min revealed no significant changes for any of the coated samples, demonstrating good initial stability of the EC coating upon exposure to liquid water. Above this time, a sinking-in behaviour was observed, with a progressive decrease of contact angle, due to water uptake by the beads (Fig. 3d). SEM images (Fig. 2) of the inner regions of the beads confirm that the coating material did not penetrate the interior, regardless of the EC concentration. Despite this, the BET analyses indicated that the coating strategy largely eliminated the mesoporous structure of the microaerogel beads, as evidenced by the absence of evaluable $N_2$-sorption isotherms. To clarify whether this effect originated from the presence of EC or from the solvent treatment involved in the coating step, an additional control experiment was carried out. In particular, the uncoated microaerogel beads were exposed to EC-free ethanol and then supercritical-$CO_2$-dried. In this case as well, the beads lost their accessible surface area, showing that the disappearance of mesoporosity was caused by the quick evaporation of ethanol and not by the presence of EC. This observation is consistent with the well-known susceptibility of aerogel mesostructures to collapse during evaporative or ambient-pressure drying due to capillary forces (Takeshita et al., 2025; Zhao et al., 2018). While mesoporosity was diminished, the macroporous architecture remained unchanged (Fig. 2), preserving the characteristic open-porous structure of the beads.

### 3.3. Vanillin release from microaerogel beads

The last part of the work focused on the evaluation of the efficacy of EC coating in controlling vanillin release from the microaerogel beads. To this aim, the microaerogel beads were loaded with vanillin through supercritical-$CO_2$ impregnation. The impregnation loading was of 21 g/100 g bead and resulted in a rougher surface appearance of the dried microaggregates within the beads (Fig. 4).

$N_2$ physisorption measurements did not yield evaluable isotherms after vanillin loading, and the BET surface area could not be reliably determined. This behaviour indicates that vanillin loading made mesopores less accessible for $N_2$ sorption. The loaded beads were then coated with the EC solutions and tested for vanillin release in water (Fig. 5).

The uncoated beads displayed a fast vanillin release, which reached a plateau after approximately 60 min of contact with water (Fig. 5), probably due to fast water absorption and bead swelling (De Berardinis et al., 2024b; García-González et al., 2021; Kéri et al., 2020; Kleemann

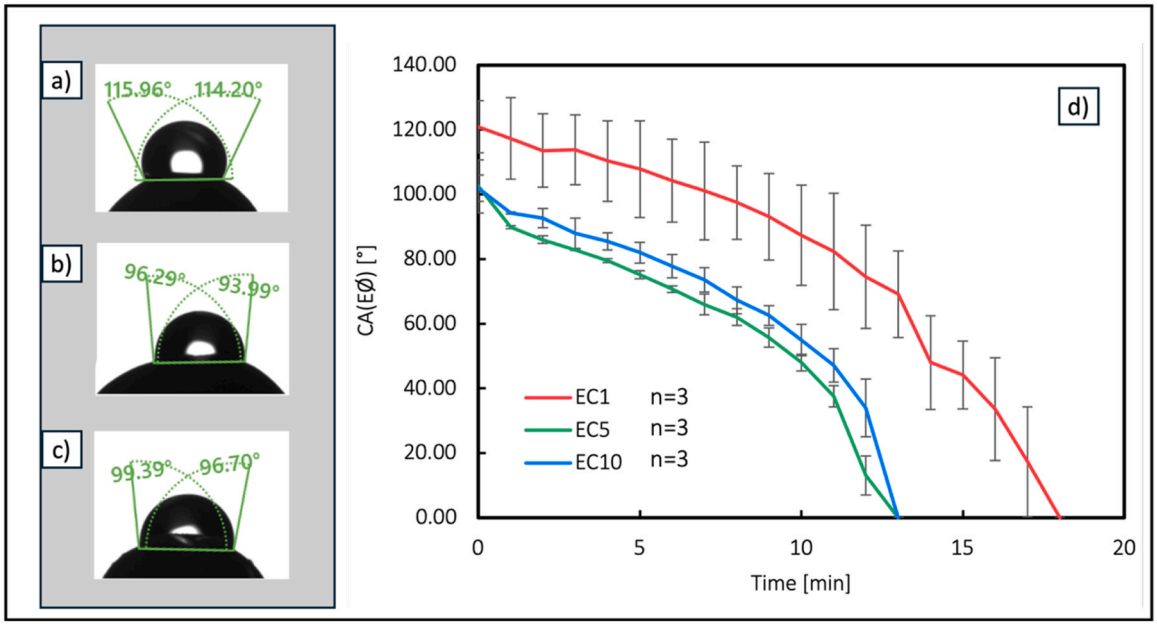


**Fig. 3.** Initial contact angle (CA) of microaerogel beads (representative images) coated by dipping in ethylcellulose solutions (EC) at increasing concentration: a) 1 g/100 g; b) 5 g/100 g; c) 10 g/100 and d) evolution of contact angle over 18 min.

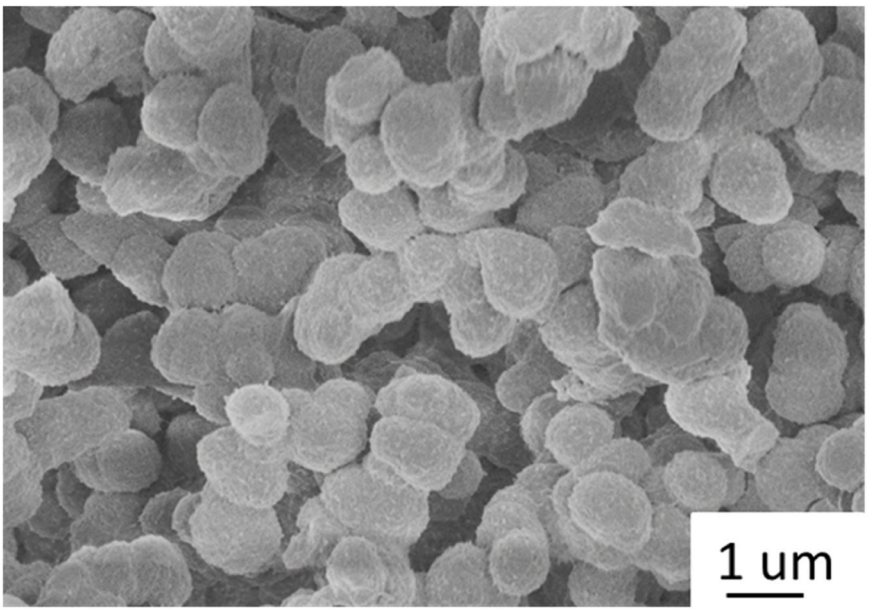


**Fig. 4.** Microstructure of the inner part of microaerogel beads loaded with vanillin.

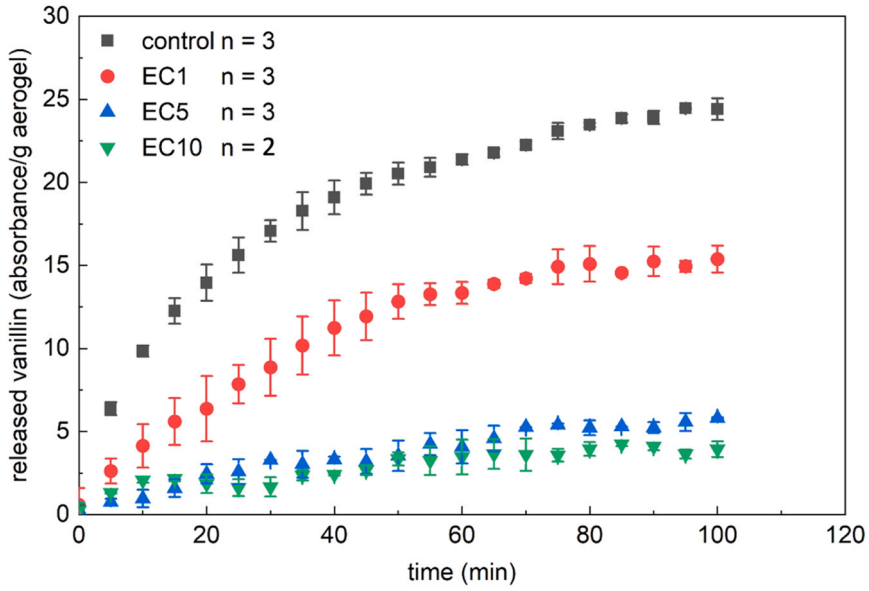


**Fig. 5.** Vanillin released from uncoated whey protein microaerogel beads (control) and from beads coated by dipping in ethylcellulose solutions (EC) at increasing concentration (1, 5, 10 g/100 g). n refers to the number of replicates, error bars correspond to the standard deviation.

et al., 2020). In contrast, the EC-coated beads displayed a markedly reduced vanillin release, with the release profiles progressively shifting towards lower values as the coating concentration increased (Fig. 5). Notably, beads coated with 5 and 10 g/100 g EC solutions showed comparable release behaviour. These findings are in accordance with those of Schroeter et al. (2021), wherein aerogel particles coated with shellac, a hydrophobic surface layer, demonstrated a notable reduction in vanillin release in comparison to the uncoated ones.

As shown in Fig. 6, vanillin release from non-coated beads exhibited a characteristic biphasic profile, which was accurately captured by a two-compartment burst–diffusion model (Eq. 1; $R^2$ 0.991):

$$c_{t,\ norm.} = f_b\left(1 - e^{-k_b \bullet t}\right) + (1 - f_b) \bullet \left(1 - e^{-k_d \cdot t}\right) \quad (1)$$

with $c_{t,\ norm.}$ being the amount of vanillin release at the time (normalized on the final amount released at the end of the release experiment), $f_b$ = 0.63 being the fraction of vanillin that is readily accessible for immediate release, i.e., the portion liberated without substantial diffusional resistance. The parameter $k_b = 6.4 \cdot 10^{-2} \pm 3.7 \cdot 10^{-3}$ $min^{-1}$ quantifies the rapid initial release phase, while $k_d = 2.4 \cdot 10^{-2} \pm 1.5 \cdot 10^{-3}$ $min^{-1}$ characterizes the subsequent, slower diffusion-controlled stage of the process.

While the two-compartment burst–diffusion model adequately described the release from non-coated beads, it did not provide a robust fit for coated formulations, where the release profile deviated from a distinct biphasic behaviour. For the kinetic description of release from coated samples, it is important to consider that the mesoporosity was diminished upon coating, while the macroporous architecture remained unchanged, preserving the characteristic open structure of the beads (see 3.2). The mesopore collapse may have contributed to partial immobilization of vanillin within the matrix, acting as a form of

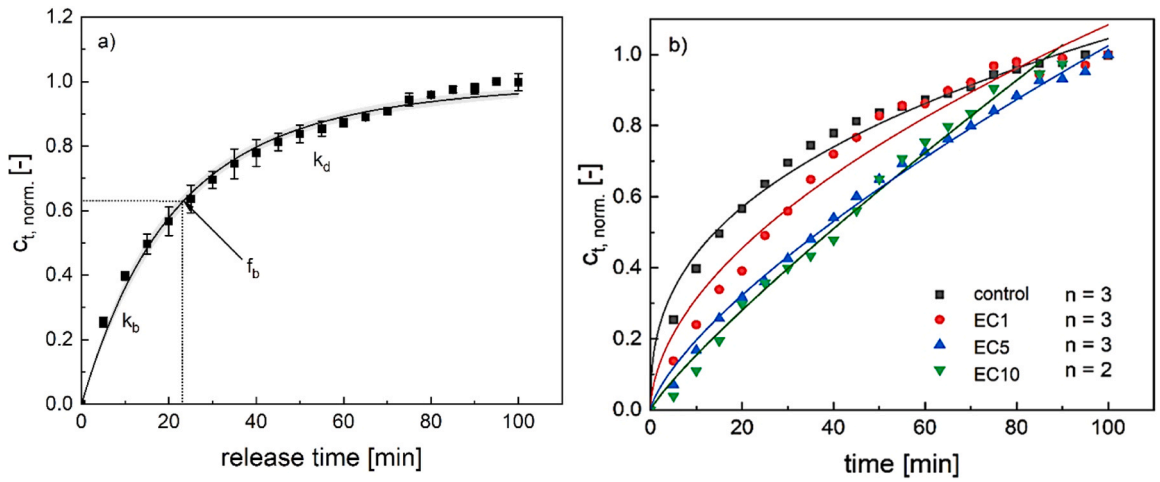


**Fig. 6.** a) Description of vanillin release from uncoated whey protein beads (control) and description of release kinetics *via* biphasic diffusion model. The straight line represents the model fit and the hatched area the 95% confidence interval. b) normalized vanillin release profiles from uncoated whey protein microaerogel beads (control) and from beads coated by dipping in ethylcellulose solutions (EC) at increasing concentration (1, 5, 10 g/100 g). Straight lines represent Korsmeyer-Peppas fits. n corresponds to the number of replicates.

structural entrapment phenomenon that could contribute to its controlled release. In this context, the comparison between the uncoated beads and those coated with the 1 g/100 g EC solution is particularly informative, as neither system exhibited a continuous external barrier that would impede mass transport. The slower release observed in samples coated with the 1 g/100 g EC solution, therefore, cannot be attributed to diffusion resistance at the bead surface. Instead, it is likely related to the partial entrapment of vanillin caused by mesopore collapse during solvent evaporation, which may have enhanced its immobilization within the matrix and delayed its diffusion into the surrounding medium.

A quantitative comparison of release kinetics between all samples was obtained by empirical fitting using the Korsmeyer–Peppas model, while the model exponent provides qualitative guidance for comparing release behaviour between samples t (Eq. 2):

$$c_{t,norm.} = kt^n \quad (2)$$

with $k$ ($min^{-1}$) being the release constant and $n$ the release exponent. The latter indicated whether transport is diffusion-controlled, swelling-controlled, or involves multiple processes. It is notable that classification of the release mechanism according to Korsmeyer–Peppas exponent thresholds is specific to the release matrix geometry (in our case: spherical). Table 1 reports the Korsmeyer- Peppas parameters for the different samples.

The release exponent ($n = 0.38$) of the uncoated control sample confirmed a Fickian diffusion mechanism. Applying a coating by dipping into a 1 g/100 g EC solution reduced the release rate constant by approximately half, although no continuous barrier layer formed at this concentration (Fig. 2). The corresponding exponent ($n = 0.54$) still reflected diffusion-controlled transport, indicating that the observed deceleration was primarily associated with partial vanillin entrapment resulting from mesopore collapse, rather than with surface-induced mass-transfer resistance. In contrast, beads coated with 5 and 10 g/100 g EC solutions exhibited markedly slower release kinetics, reflected by a substantial reduction in $k$. For these samples, the exponents increased to $n = 0.72$ and $n = 0.86$, respectively, indicating a transition from anomalous transport (combined diffusion and polymer relaxation) towards Case-II-like behaviour dominated by barrier-controlled release. Owing to the near-insolubility of the EC layer in aqueous media, this closed coating structure (Fig. 2) acted as an effective diffusion barrier. Taken together, the Korsmeyer-Peppas parameters clearly reflected the shift in dominant release mechanism as the EC concentration increased: from purely diffusion-driven release in uncoated beads, to mixed or swelling-affected transport at intermediate coating levels, and finally to barrier-controlled Case-II transport when a uniform, hydrophobic shell is established. This mechanistic evolution corroborates the release curves and demonstrates the strong modulatory effect of EC coating thickness on vanillin release dynamics.

**Table 1**
Korsmeyer-Peppas parameters for uncoated whey protein beads (control) and beads coated by dipping in ethylcellulose solutions (EC) at increasing concentration (1, 5, 10 g/100 g).

| EC (g/100 g) | $R^2$ | $k$ ($min^{-1}$) | $n$ | Indicated mechanism |
|---|---|---|---|---|
| Control | 0.985 | 0.185 ± 0.012 | 0.38 ± 0.02 | Fickian diffusion |
| 1 | 0.966 | 0.090 ± 0.013 | 0.54 ± 0.03 | Fickian diffusion |
| 5 | 0.995 | 0.038 ± 0.003 | 0.72 ± 0.02 | anomalous transport |
| 10 | 0.991 | 0.021 ± 0.003 | 0.86 ± 0.03 | case II transport |

## 4. Conclusions

In this study, whey protein microaerogel beads impregnated with vanillin were developed for controlled delivery of this bioactive aroma compound in food. The beads were successfully coated by dipping into ethylcellulose (EC) solutions, providing a simple approach to modify surface properties and vanillin release behaviour. Increasing the EC concentration in the coating solution resulted in thicker and more homogeneous coating layers, accompanied by a loss of mesoporosity. These structural changes translated directly into altered release characteristics. While uncoated microaerogel beads exhibited rapid, predominantly Fickian diffusion of vanillin, progressively thicker EC coatings led to reduced release rates and delayed release profiles, indicating a transition toward barrier-controlled mass transfer.

These findings demonstrate that the EC coating plays a decisive role in modulating release kinetics, enabling a tunable release behaviour through straightforward adjustment of coating conditions. Importantly, the applied coating strategy allows the decoupling of aerogel particle formation and subsequent coating, offering flexibility for the design of functional delivery systems.

Future research should focus on alternative coating approaches able to reduce the loss of loaded bioactives due to diffusion into the dipping solution. In this regard, a feasible and scalable alternative to dip-coating is represented by spray-coating of aerogel beads, involving localized surface deposition of the coating solution, potentially reducing vanillin

diffusion out of the beads.

Also, further work should investigate the performance of the coated microaerogel beads in real food matrices. Indeed, common processing conditions (e.g., heating, freezing, mixing, shearing) in the presence of different food matrix components (e.g., lipids, proteins, and water) should be evaluated, as they may influence both the structure of the beads and the release of the loaded compounds. Finally, comprehensive sensory and digestibility studies of foods containing the beads loaded with aroma/bioactive compounds will be essential to evaluate the aroma release kinetics during the eating experience and their digestive fate.

## CRediT authorship contribution statement

**Lorenzo De Berardinis:** Writing – review & editing, Writing – original draft, Visualization, Methodology, Investigation, Formal analysis, Data curation. **Stella Plazzotta:** Writing – review & editing, Visualization, Methodology, Investigation, Formal analysis, Data curation, Conceptualization. **Baldur Schroeter:** Writing – review & editing, Visualization, Methodology, Investigation, Formal analysis, Data curation, Conceptualization. **Alberto Saitta:** Writing – review & editing, Formal analysis. **Irina Smirnova:** Writing – review & editing, Supervision, Resources. **Lara Manzocco:** Writing – review & editing, Supervision, Resources, Project administration, Conceptualization.

## Funding

This publication is based upon work from IG-COST Action “Technical, commercial and societal innovations on aerogels towards circular economy (IG18125)”, supported by COST (European Cooperation in Science and Technology).

Publication produced with funding from the project “Cooperazione transfrontaliera per la valorizzazione di piante alpine fonte di composti bioattivi” (NETTLE) – codice progetto “ITAT−11–007”, programma: “PC Interreg Italia Austria 2021–2027”.

## Declaration of Competing Interest

The authors declare that they have no known competing financial interests or personal relationships that could have appeared to influence the work reported in this paper.

## Data Availability

Data will be made available on request.

## References

Ahmadi, M., Madadlou, A., & Saboury, A. A. (2016). Whey protein aerogel as blended with cellulose crystalline particles or loaded with fish oil. *Food Chemistry, 196*, 1016–1022. https://doi.org/10.1016/j.foodchem.2015.10.031

Almeida, A. R. R. P., Freitas, V. L. S., Campos, J. I. S., Ribeiro da Silva, M. D. M. C., & Monte, M. J. S. (2019). Volatility and thermodynamic stability of vanillin. *The Journal of Chemical Thermodynamics, 128*, 45–54. https://doi.org/10.1016/j.jct.2018.07.023

Betz, M., García-González, C. A., Subrahmanyam, R. P., Smirnova, I., & Kulozik, U. (2012). Preparation of novel whey protein-based aerogels as drug carriers for life science applications. *The Journal of Supercritical Fluids, 72*, 111–119. https://doi.org/10.1016/j.supflu.2012.08.019

Ciufarrin, F., Plazzotta, S., Rondou, K., Van Bockstaele, F., Dewettinck, K., Manzocco, L., & Calligaris, S. (2024). Oil structuring using whey protein-based cryogel particles: Effect of gelation pH and feasibility as an ingredient in low-saturated fat cocoa spreads. *Food Research International, 196*, Article 115029. https://doi.org/10.1016/j.foodres.2024.115029

Comin, L. M., Temelli, F., & Saldaña, M. D. A. (2012). Barley β-glucan aerogels as a carrier for flax oil via supercritical CO2. *Journal of Food Engineering, 111*, 625–631. https://doi.org/10.1016/j.jfoodeng.2012.03.005

De Berardinis, L., Plazzotta, S., Magnan, M., & Manzocco, L. (2024a). Hybrid aerogels of spirulin and whey proteins as novel cellular solids. *LWT, 213*, Article 117078. https://doi.org/10.1016/j.lwt.2024.117078

De Berardinis, L., Plazzotta, S., Magnan, M., & Manzocco, L. (2024b). Hydrophilic or hydrophobic coating of whey protein aerogels obtained by supercritical-CO2-drying: Effect on physical properties, moisture adsorption and interaction with water and oil in food systems. *Innovative Food Science & Emerging Technologies, 91*, Article 103530. https://doi.org/10.1016/j.ifset.2023.103530

de Oliveira, J. P., Bruni, G. P., Fonseca, L. M., da Silva, F. T., da Rocha, J. C., & da Rosa Zavareze, E. (2020). Characterization of aerogels as bioactive delivery vehicles produced through the valorization of yerba-mate (Ilex paraguariensis paraguariensis). *Food Hydrocolloids, 107*, Article 105931. https://doi.org/10.1016/j.foodhyd.2020.105931

dos Santos, P., Viganó, J., Furtado, G., de, F., Cunha, R. L., Hubinger, M. D., Rezende, C. A., & Martínez, J. (2020). Production of resveratrol loaded alginate aerogel: Characterization, mathematical modeling, and study of impregnation. *The Journal of Supercritical Fluids, 163*, Article 104882. https://doi.org/10.1016/j.supflu.2020.104882

García-González, C. A., Budtova, T., Durães, L., Gaudio, P. Del, Gurikov, P., Koebel, M., Liebner, F., Neagu, M., & Smirnova, I. (2019). An opinion paper on aerogels for biomedical and environmental applications. *Molecules, 24*, 1815. https://doi.org/10.3390/molecules24091815

García-González, C. A., & Smirnova, I. (2013). Use of supercritical fluid technology for the production of tailor-made aerogel particles for delivery systems. *Journal of Supercritical Fluids, 79*. https://doi.org/10.1016/j.supflu.2013.03.001

García-González, C. A., Sosnik, A., Kalmár, J., De Marco, I., Erkey, C., Concheiro, A., & Alvarez-Lorenzo, C. (2021). Aerogels in drug delivery: From design to application. *Journal of Controlled Release, 332*, 40–63. https://doi.org/10.1016/j.jconrel.2021.02.012

Goslinska, M., Selmer, I., Kleemann, C., Kulozik, U., Smirnova, I., & Heinrich, S. (2019). Novel technique for measurement of coating layer thickness of fine and porous particles using focused ion beam. *Particuology, 42*, 190–198. https://doi.org/10.1016/j.partic.2018.03.002

IUPAC. (2022). *IUPAC Announces the 2022 Top Ten Emerging Technologies in Chemistry - IUPAC | International Union of Pure and Applied Chemistry*. ⟨https://iupac.org/iupac-2022-top-ten/⟩.

Jung, I., Schroeter, B., Plazzotta, S., De Berardinis, L., Smirnova, I., Gurikov, P., & Manzocco, L. (2023). Oleogels from mesoporous whey and potato protein based aerogel microparticles: Influence of microstructural properties on oleogelation ability. *Food Hydrocolloids, 142*, Article 108758. https://doi.org/10.1016/j.foodhyd.2023.108758

Kéri, M., Forgács, A., Papp, V., Bányai, I., Veres, P., Len, A., Dudás, Z., Fábián, I., & Kalmár, J. (2020). Gelatin content governs hydration induced structural changes in silica-gelatin hybrid aerogels – Implications in drug delivery. *Acta Biomaterialia, 105*, 131–145. https://doi.org/10.1016/j.actbio.2020.01.016

Kleemann, C., Schuster, R., Rosenecker, E., Selmer, I., Smirnova, I., & Kulozik, U. (2020). In-vitro-digestion and swelling kinetics of whey protein, egg white protein and sodium caseinate aerogels. *Food Hydrocolloids, 101*, Article 105534. https://doi.org/10.1016/j.foodhyd.2019.105534

Manzocco, L., Mikkonen, K. S., & García-González, C. A. (2021). Aerogels as porous structures for food applications: smart ingredients and novel packaging materials. *Food Structure, 28*, Article 100188. https://doi.org/10.1016/j.foostr.2021.100188

Manzocco, L., Plazzotta, S., Powell, J., de Vries, A., Rousseau, D., & Calligaris, S. (2022). Structural characterisation and sorption capability of whey protein aerogels obtained by freeze-drying or supercritical drying. *Food Hydrocolloids, 122*, Article 107117. https://doi.org/10.1016/j.foodhyd.2021.107117

Manzocco, L., Valoppi, F., Calligaris, S., Andreatta, F., Spilimbergo, S., & Nicoli, M. C. (2017). Exploitation of κ-carrageenan aerogels as template for edible oleogel preparation. *Food Hydrocolloids, 71*, 68–75. https://doi.org/10.1016/.foodhyd.2017.04.021

Méndez, D. A., Schroeter, B., Martínez-Abad, A., Fabra, M. J., Gurikov, P., & López-Rubio, A. (2023). Pectin-based aerogel particles for drug delivery: Effect of pectin composition on aerogel structure and release properties. *Carbohydrate Polymers, 306*, Article 120604. https://doi.org/10.1016/j.carbpol.2023.120604

Miguel, F., Martín, A., Gamse, T., & Cocero, M. J. (2006). Supercritical anti solvent precipitation of lycopene: Effect of the operating parameters. *The Journal of Supercritical Fluids, 36*, 225–235. https://doi.org/10.1016/j.supflu.2005.06.009

Nicolai, T. (2016). Formation and functionality of self-assembled whey protein microgels. *Colloids and Surfaces B, Biointerfaces, 137*, 32–38. https://doi.org/10.1016/j.colsurfb.2015.05.055

Olatunde, A., Mohammed, A., Ibrahim, M. A., Tajuddeen, N., & Shuaibu, M. N. (2022). Vanillin: A food additive with multiple biological activities. *European Journal of Medicinal Chemistry Reports, 5*, Article 100055. https://doi.org/10.1016/j.ejmcr.2022.100055

Plazzotta, S., Alongi, M., De Berardinis, L., Melchior, S., Calligaris, S., & Manzocco, L. (2022). Steering protein and lipid digestibility by oleogelation with protein aerogels. *Food & Function, 13*, 10601–10609. https://doi.org/10.1039/d2fo01257j

Plazzotta, S., Calligaris, S., & Manzocco, L. (2020). Structural characterization of oleogels from whey protein aerogel particles. *Food Research International, 132*, Article 109099. https://doi.org/10.1016/j.foodres.2020.109099

Plazzotta, S., Jung, I., Schroeter, B., Subrahmanyam, R. P., Smirnova, I., Calligaris, S., Gurikov, P., & Manzocco, L. (2021). Conversion of whey protein aerogel particles into oleogels: Effect of oil type on structural features. *Polymers, 13*, 4063. https://doi.org/10.3390/polym13234063/S1

Schroeter, B., Yonkova, V. P., Goslinska, M., Orth, M., Pietsch, S., Gurikov, P., Smirnova, I., & Heinrich, S. (2021). Spray coating of cellulose aerogel particles in a miniaturized spouted bed. *Cellulose, 28*, 7795–7812. https://doi.org/10.1007/s10570-021-04032-0

Selmer, I., Karnetzke, J., Kleemann, C., Lehtonen, M., Mikkonen, K. S., Kulozik, U., & Smirnova, I. (2019). Encapsulation of fish oil in protein aerogel micro-particles. *Journal of Food Engineering, 260*, 1–11. https://doi.org/10.1016/j.jfoodeng.2019.04.016

Smirnova, I., & Gurikov, P. (2018). Aerogel production: Current status, research directions, and future opportunities. *The Journal of Supercritical Fluids, 134*, 228–233. https://doi.org/10.1016/j.supflu.2017.12.037

Takeshita, S., Mine, S., & Ono, T. (2025). Data-Driven Review on Aerogels and Polymeric Aerogels. *Angewandte Chemie International Edition, 64*(28), Article e202504250. https://doi.org/10.1002/anie.202504250

Thommes, M., Kaneko, K., Neimark, A. V., Olivier, J. P., Rodriguez-Reinoso, F., Rouquerol, J., & Sing, K. S. W. (2015). Physisorption of gases, with special reference to the evaluation of surface area and pore size distribution (IUPAC Technical Report). *Pure and Applied Chemistry, 87*, 1051–1069. https://doi.org/10.1515/PAC-2014-1117/ASSET/GRAPHIC/J_PAC-2014-1117_FIG_010.JPG

Ubeyitogullari, A., & Ciftci, O. N. (2017). Generating phytosterol nanoparticles in nanoporous bioaerogels via supercritical carbon dioxide impregnation: Effect of impregnation conditions. *Journal of Food Engineering, 207*, 99–107. https://doi.org/10.1016/j.jfoodeng.2017.03.022

Ubeyitogullari, A., & Ciftci, O. N. (2019). vitro bioaccessibility of novel low-crystallinity phytosterol nanoparticles in non-fat and regular-fat foods. *Food Research International, 123*, 27–35. https://doi.org/10.1016/j.foodres.2019.04.014

Zhao, S., Malfait, W. J., Guerrero-Alburquerque, N., Koebel, M. M., & Nyström, G. (2018). Biopolymer aerogels and foams: Chemistry, properties, and applications. *Angewandte Chemie International Edition, 57*, (26), 7580–7608. https://doi.org/10.1002/ange.201709014